

# Alcohol extract of *Rubia yunnanensis*: Metabolic alterations and preventive effects against OGD/R-induced oxidative damage in HT22 cells

JIANGHAO CHENG, GAOYIZHOU LI, LIPING YANG, PU CHEN and XIAOHUA DUAN

Yunnan Key Laboratory of Dai and Yi Medicines, Yunnan University of Chinese Medicine, Kunming, Yunnan 650500, P.R. China

Received January 8, 2024; Accepted February 28, 2024

DOI: 10.3892/br.2024.1763

**Abstract.** The present study investigated the inhibitory and neuroprotective effects of *Rubia yunnanensis* alcohol extract (RY-A) on oxidative stress induced by oxygen-glucose deprivation/reoxygenation (OGD/R) in HT22 cells. *In vitro* cultured HT22 cells were randomly divided into control, OGD/R, OGD/R + 100  $\mu\text{mol/l}$  edaravone and OGD/R + 10, 20 and 40  $\mu\text{g/ml}$  RY-A groups. Oxygen-sugar deprivation was performed with 10 mmol/l sodium dithionite combined with sugar-free DMEM medium for 2 h, followed by re-glycolization and reoxygenation for 2 h to establish an *in vitro* OGD/R model. Cell morphology was observed under a phase contrast microscope. Cell survival rate was detected by thiazolyl blue and lactate dehydrogenase and oxidative stress-related indexes were detected by commercial kits. The effects and metabolic alterations of RY-A treatment after OGD/R were evaluated using ultra-high performance liquid chromatography and mass spectrometry. Protein levels were further examined by western blotting. The results showed that cells in the OGD/R group were swollen and lacked protrusions, had significantly reduced viability and had significantly elevated oxidative stress-related indexes of reactive oxygen species, nitric oxide levels and malondialdehyde content and significantly reduced activities of the antioxidant enzymes superoxide dismutase and glutathione peroxidase, compared with controls. Compared with the OGD/R group, the RY-A group had significantly improved cell morphology and significantly increased cell viability and in terms of oxidative stress, exhibited significantly reduced reactive oxygen species, nitric oxide levels and

malondialdehyde content, as well as significantly increased superoxide dismutase and glutathione peroxidase activities. Metabolomic analysis identified changes in 20 metabolites, including L-tryptophan, ornithine, eicosapentaenoic acid-d5, isosafrole and xanthine. Metabolomics analysis showed that the pathways affected included those related to phenylalanine, tyrosine and tryptophan biosynthesis, the prolactin signaling pathway and amphetamine addiction. These results suggested that RY-A had significant preventive effects on an *in vitro* model of cerebral ischemia-reperfusion injury simulated by OGD/R and the mechanism may be related to increased tryptophan content, activation of indoleamine 2,3-dioxygenase enzymes and inhibition of oxidative stress.

## Introduction

Stroke is the second most common mortality among global diseases, with ischemic stroke accounting for 85% of cases (1-3). One of the most effective treatments for acute ischemic stroke is intravenous thrombolytic therapy (4). However, thrombolytic therapy is often accompanied by side effects or aggravation. Vascular recanalization induces a series of pathological processes to varying degrees, such as oxidative stress, inflammation and peripheral immune cell infiltration, leading to neuronal cell death near the lesion; clinically known as cerebral ischemia reperfusion injury (CIRI). Vascular recanalization also triggers transient or permanent neurological dysfunctional diseases such as vascular dementia (5-7). Therefore, to protect brain tissue from ischemia-reperfusion injury and further improve functional prognosis, the development of neuroprotective drugs is urgently needed for patients with ischemic stroke after thrombolytic therapy.

Traditional Chinese medicine has a multi-target, multi-pathway compound effect and its monomer preparations are characterized by small side effects and significant therapeutic effects (8). Such features allow the treatment of ischemic stroke by traditional Chinese medicine to have great potential for its application in a wide range of diseases. Herbs from Yunnan are widely used in the prevention and treatment of cardiovascular, gastrointestinal and traumatic diseases and they have been documented in the 'Southern Yunnan Materia Medica' and applied for hundreds of years (9). One of these

---

Correspondence to: Dr Xiaohua Duan, Yunnan Key Laboratory of Dai and Yi Medicines, Yunnan University of Chinese Medicine, 1076 Yuhua Road, Chenggong, Kunming, Yunnan 650500, P.R. China  
E-mail: 1047896527@qq.com

**Key words:** *Rubia yunnanensis*, oxygen-glucose deprivation/reoxygenation, HT22 cells, oxidative stress, indoleamine 2,3-dioxygenase enzymes, MAPK pathway

herbs, *Rubia yunnanensis*, is the dried root and rhizome of *Rubia yunnanensis* Diels (a plant of the *Rubiaceae* family) and is an indigenous medicine endemic to Yunnan, China. *Rubia yunnanensis* has pharmacological effects, such as anti-oxidation, anti-ischemia and anti-thrombosis actions (10). *Rubia yunnanensis* was commonly used by some famous Chinese doctors, such as Zhang Chao, a famous Chinese medicine practitioner in Yunnan Province, to treat certain cerebral ischemic disorders, such as dizziness and anemia caused by cerebral ischemia. Some Chinese medicine practitioners also commonly use *Rubia yunnanensis* to treat dizziness and anemia. This application suggests that *Rubia yunnanensis* may have the potential to treat ischemic stroke and subsequent validation in more direct human trials may lead to the gradual clinical application of *Rubia yunnanensis*. HT22 cells that lack the N-methyl-D-aspartic acid receptor are the most commonly used *in vitro* cell model in oxidative stress-related studies. By exploring the potential therapeutic effects and mechanisms of the *Rubia yunnanensis*, new ideas and methods may be provided for the prevention and treatment of ischemic stroke.

In terms of the innovative aspects of the present study, it demonstrated the antioxidant protective effect of RY-A in mouse hippocampal HT22 cells used as an oxygen-glucose deprivation/reoxygenation (OGD/R) model, investigated the metabolic alterations between OGD/R and RY-A groups using a metabolomics approach and explored the involvement of MAPK signaling pathways in its molecular mechanism. The results suggested that RY-A may be a potentially effective therapeutic herb for patients with CIRI.

## Materials and methods

*Preparation of the alcohol extract of Rubia yunnanensis.* *Rubia yunnanensis* was purchased from Yunnan Huide Pharmaceutical Co., Ltd. and was identified by Professor Zili Yin of Yunnan University of Traditional Chinese Medicine (Yunnan, China). The alcohol extract of *Rubia yunnanensis* was obtained by soaking 500 g of powdered *Rubia yunnanensis* in 95% ethanol for 24 h. Heating and refluxing at 60°C, then repeatedly soaking, heating and refluxing for four times to obtain the alcohol extract of *Rubia yunnanensis*.

*Cell cultivation and preparation of the OGD/R model.* HT22 cells (Shanghai Enzyme Research Biotechnology Co., Ltd.) were derived from the mouse hippocampal neuronal cell line. HT22 cells were cultured in high glucose DMEM (cat. no. 2024059) containing 10% fetal bovine serum (cat. no. 04-001-1A) and 1% penicillin-streptomycin (cat. no. 2114092; all from Biological Industries) and were routinely passaged in an incubator at 37°C and, 5% CO<sub>2</sub>. The cells were cultured in 96-well plates at a density of 1x10<sup>5</sup>/ml for 24 h during the logarithmic growth period and then grouped. *In vitro* cultured HT22 cells were randomly divided into control group, OGD/R group, OGD/R group, OGD/R + 100 μmol/l edaravone (Beijing Solarbio Science & Technology Co., Ltd.; EDA group) and OGD/R + 10, 20, or 40 μg/ml RY-A (RY-A group). The control group was left untreated and the OGD/R group was cultured in oxygen/sugar deprivation conditions for 2 h in sugar-free DMEM medium (11) containing 10 mmol/l Na<sub>2</sub>S<sub>2</sub>O<sub>4</sub> (cat. no. 2029548; Biological Industries) and was

then cultured in serum-free high-sugar DMEM for 2 h for reconstitution. Cells were incubated in DMEM for 2 h for reoxygenation to establish an *in vitro* OGD/R model. The EDA and RY-A were added at final concentrations starting 24 h before oxygen deprivation and until the end of reoxygenation.

*Cell viability assay.* HT22 cells were routinely cultured in 96-well plates at a density of 1x10<sup>5</sup>/ml during the logarithmic growth phase for 24 h. After treating the cells in each group according to the aforementioned methods, 20 μl thiazolyl blue tetrazolium bromide (MTT; 5 mg/ml; Shanghai Suoqiao Biotech Co., Ltd.) was added to each well and incubated at 37°C for 4 h. The liquid in the wells was carefully pipetted off and 150 μl of dimethyl sulfoxide solution was added. Wells were shaken at low speed for 5 min until the crystals were completely dissolved. Absorbance was measured at 490 nm on an enzyme labeling instrument (VariosKan Flash; Thermo Fisher Scientific, Inc.).

*Cell mortality assay.* The cell culture conditions and grouping were unchanged and 96-well plates were used. After 2 h of sugar restoration and reoxygenation, the original medium was replaced by 200 μl/well of serum-free medium and the cell mortality rate was detected according to the specifications of a lactate dehydrogenase (LDH) Cytotoxicity Detection Kit (cat. no. C0016, Shanghai Biyuntian Biotechnology Co., Ltd.).

*Detection of intracellular reactive oxygen species (ROS) levels.* HT22 cells were routinely cultured and ROS levels were detected using a ROS detection kit (cat. no. S0033S; Shanghai Biyuntian Biotechnology Co., Ltd.). Cells were cultured in 6-well plates at a density of 6.5x10<sup>4</sup>/ml during the logarithmic growth phase for 24 h. After treating the cells in each group according to the aforementioned methods, 20 min before the end of the treatment, dichlorodihydrofluorescein diacetate was added to each well at a ratio of 1:1,000 and aspirated well to make complete contact between the probes and cells. The cells were incubated at 37°C for 20 min and then washed three times with phosphate-buffered saline. The fluorescence intensity was detected in an enzyme labeling instrument (VariosKan Flash; Thermo Fisher Scientific, Inc.) using 488 nm excitation wavelength and 525 nm emission wavelength.

*Determination of nitric oxide (NO) and malondialdehyde (MDA) content and superoxide dismutase (SOD) and glutathione peroxidase (GSH-Px) activities.* HT22 cells were routinely cultured in 6-well plates for 24 h at a density of 6.5x10<sup>4</sup>/ml during the logarithmic growth phase. After treating the cells in each group, the cells were analyzed according to the BCA Protein Concentration Assay Kit (cat. no. P0010), Nitric oxide (NO) Detection Kit (cat. no. S0021S), Malondialdehyde (MDA) Detection Kit (cat. no. S0131S), Superoxide dismutase (SOD) Detection Kit (cat. no. S0101S) and Glutathione peroxidase (GSH-Px) kit (cat. no. S0057S; Shanghai Biyuntian Biotechnology Co., Ltd.) for the determination of NO, MDA, SOD and GSH-Px.

*Metabolomics assay.* HT22 cells were routinely cultured at a density of 6.5x10<sup>4</sup>/ml during the logarithmic growth phase in 6-well plates for 24 h. Cells were divided into the OGD/R and

RY-A (OGD/R + 20  $\mu\text{g/ml}$  RY-A) groups, with one sample/two wells and six samples of each collected for analysis.

The cell sample was pipetted into a 2 ml centrifuge tube and 100 mg of glass beads added. Acetonitrile:methanol:H<sub>2</sub>O (1,000  $\mu\text{l}$ ; 2:2:1, v:v:v) was added and the sample vortexed for 30 sec. The tube was placed in the 2 ml adapter and frozen in liquid nitrogen for 5 min. The tube was removed and thawed at room temperature. The tube was then placed again in the 2 ml adapter and mounted in the tissue grinder and ground at 60 Hz for 2 min, repeated twice. The tube was removed and centrifuged at 14,000  $\times$  g for 10 min at 4°C. The supernatant was concentrated and dried. The sample was reconstituted by adding exactly 300  $\mu\text{l}$  of 2-chloro-L-phenylalanine (4 ppm) solution in acetonitrile:0.1% formic acid (1:9; v:v) and the supernatant was filtered through a 0.22  $\mu\text{m}$  membrane. The filtrate was added to the assay vial and used for ultra-high performance liquid chromatography (UHPLC) and mass spectrometry (MS) detection.

#### UHPLC-MS conditions

**UHPLC conditions.** A Thermo Vanquish (Thermo Fisher Scientific, Inc.) UHPLC system was used with an ACQUITY UPLC HSS T3 (2.1 $\times$ 100 mm, 1.8  $\mu\text{m}$ ; Waters Corporation) column. The flow rate was 0.3 ml/min, the column temperature was 40°C and the injection volume was 2  $\mu\text{l}$ . The mobile phases were 0.1% formic acid in acetonitrile (B2) and 0.1% formic acid with water (A2) in positive ionization mode and the gradient elution program was as follows: 0-1 min, 8% B2; 1-8 min, 8-98% B2; 8-10 min, 98% B2; 10-10.1 min, 98-8% B2; 10.1-12 min, 8% B2. In negative ionization mode, the mobile phases were acetonitrile (B3) and 5 mM ammonium formate in water (A3) and the gradient elution program was: 0-1 min, 8% B3; 1-8 min, 8-98% B3; 8-10 min, 98% B3; 10-10.1 min, 98-8% B3; and 10.1-12 min, 8% B3 (12).

**MS conditions.** Data were acquired separately in positive and negative ion mode on a Thermo Orbitrap Exploris 120 MS detector (Thermo Fisher Scientific, Inc.) with an electrospray ionization source. The positive ion spray voltage was 3.50 kV, the negative ion spray voltage was -2.50 kV, the sheath gas was 40 arb and the auxiliary gas was 10 arb. The capillary temperature was 325°C and a primary full scan was performed at a resolution of 60,000, with a primary ion scanning range of 100-1,000 m/z. Secondary cleavage was performed using an HCD with a collision energy of 30% and a secondary resolution of 15,000. The first four ions of the acquired signal were fragmented, while dynamic exclusion was used to remove unnecessary MS/MS information (13).

**Metabolomics analysis.** Chromatographic data were converted to mzXML file format by the MSConvert tool in the ProteoWizard software package (v3.0.8789) (14), then the retention time correction, peak detection, peak filtering and peak alignment processes were performed by the R XCMS (v3.12.0) software package (15). The parameters were set to bw=2, ppm=15, peakwidth=c(5,30), mzwid=0.015, mzdiff=0.01 and method='centWave', resulting in a quantitative list of substances containing the retention times, mass-to-charge ratios and peak areas in data matrices. Substance identification was performed using spectral databases, such as the Human Metabolome

Database (16), Massbank (17), LipidMaps (18), Mzcloud (19), Kyoto Encyclopedia of Genes and Genomes (20) and the metabolite database build by Panomix Biomedical Tech Co., Ltd. (<http://query.biodeep.cn/>), for searching and comparing, characterization and annotation. The peak area data of metabolites were imported into the R language Ropls package (21) for multivariate statistical analysis, including principal component analysis (PCA), partial least squares-discriminant analysis (PLS-DA) and orthogonal partial least squares discriminant analysis (OPLS-DA).

The model was tested for overfitting using the replacement test. R<sup>2</sup>X and R<sup>2</sup>Y denoted the explanatory rate of the constructed model for the X and Y matrices, respectively and Q<sup>2</sup> labels the predictive power of the model. Values closer to 1 indicated that the fit of model is improved and samples in the training set can be more accurately classified into their original attributions. The P-value was calculated according to the statistical test and the variable projection importance (VIP) was calculated by the OPLS-DA dimensionality reduction method. Fold change (FC) was calculated by the multiplicity of difference between groups to measure the strength of the influence of each metabolite content on the classification discrimination of samples and the explanatory ability, which assisted in the screening of marker metabolites. Metabolite molecules were considered statistically significantly different when P<0.05 and VIP>1. Functional pathway enrichment and topological analysis of the screened differential metabolites were performed using the MetaboAnalyst software package (22).

**Western blotting to detect protein expression levels.** HT22 cells were routinely cultured in 6-well plates at a density of 6.5 $\times$ 10<sup>4</sup>/ml during the logarithmic growth phase for 24 h. After treatment of the cells in each group, the cells were lysed on ice for 20 min with RIPA (cat. no. P0013C; Beyotime Institute of Biotechnology) lysis buffer [PSMF (cat. no. MFC00007424; Amresco, LLC):RIPA lysate=1:100]. The supernatant was centrifuged at 4°C for 5 min at 12,000  $\times$  g. Protein concentration was determined by the BCA method (Beyotime Institute of Biotechnology). Total protein (80  $\mu\text{g}$ ) was separated by 8% SDS-PAGE gel electrophoresis and then transferred to a polyvinylidene difluoride membrane (0.45  $\mu\text{m}$ ; cat. no. IPFL85R; MilliporeSigma). After membrane transfer, the membrane was blocked with 5% skimmed milk powder at room temperature for 2 h. Subsequently, the cells were incubated with primary antibodies: IDO (dilution 1:1,000; cat. no. 51851; Cell Signaling Technology, Inc.), p38 (dilution 1:2,000; cat. no. 14064-1-AP; Proteintech Group, Inc.), p-p38 (dilution 1:1,000; cat. no. 28796-1-AP; Proteintech Group, Inc.), ERK1+2 antibody (dilution 1:10,000; cat. no. ab184699; Abcam), phosphorylated (p-)ERK antibody (dilution 1:1,000; cat. no. ab201015; Abcam), JNK antibody (dilution 1:1,000; cat. no. 9252; Cell Signaling Technology, Inc.), p-JNK antibody (dilution 1:1,000; cat. no. 9251; Cell Signaling Technology, Inc.),  $\beta$ -Actin (cat. no. ab8226; Abcam) overnight at 4°C, followed by incubation with secondary antibody [Goat Anti-Rabbit IgG HRP (HRP), dilution 1:10,000; cat. no. Ab6721; Rabbit Anti-Mouse IgG hanger L (HRP), dilution 1:10,000; cat. no. Ab6728; Abcam] for 2 h at room temperature. Chemiluminescence was visualized and imaged, the bands were analyzed semi-quantitatively

using an automated gel imaging system (Bio-Rad Laboratories, Inc.) and ImageJ v2 (National Institute of Health).  $\beta$ -Actin was used as a reference.

**Statistical analysis.** Data are expressed as mean  $\pm$  standard deviation (SD). Data were analyzed using GraphPad Prism 8.0 software (GraphPad Software, Inc.; Dotmatics). If the data were normally distributed with homogeneous variance, Bonferroni's multiple comparison test was performed following one-way analysis of variance (ANOVA). If the data were normally distributed but the variance was not homogeneous, Welch's ANOVA test followed by Dunnett's T3 multiple comparisons test was used.  $P < 0.05$  was considered to indicate a statistically significant difference.

## Results

**Determination of the dose-dependent actions of RY-A on HT22 cells.** HT22 cells were treated with different concentrations of RY-A for 24 h and the effect of RY-A on cell viability was detected. Compared with the control group, cell viability increased from 10 to 20  $\mu\text{g/ml}$  and decreased with increasing concentrations of RY-A from 40 to 80  $\mu\text{g/ml}$ , but there was no significant difference. After reaching 160  $\mu\text{g/ml}$  RY-A, high concentrations of RY-A resulted in a significant dose-dependent decrease in cell viability and toxic effects ( $P < 0.001$ ), as shown in Fig. 1A.

**Effect of RY-A on cell viability of OGD/R treated HT22 cells.** The MTT results showed that the cell survival rate of the OGD/R group decreased significantly and reached half lethal levels ( $P < 0.0001$ ) compared with the control group. Compared with the OGD/R group, the cell survival rate was dose-dependently increased in the range of 10–20  $\mu\text{g/ml}$  RY-A, whereas cell survival was decreased with 40  $\mu\text{g/ml}$  RY-A, yielding an optimal effective concentration of 20  $\mu\text{g/ml}$ , as shown in Fig. 1B.

**Morphology of HT22 cells.** The cells in the control group were morphologically normal, triangular, with bipolar or multipolar protrusions, large cytosol, complete and smooth cell membranes and connected into a network. After 4 h of OGD/R treatment, the number of cells in the OGD/R group was significantly reduced and most of the cells lost their protrusions and were rounded. However, the effects of OGD/R were significantly reversed by RY-A pretreatment, as shown in Fig. 1C.

**Effect of RY-A on LDH release and oxidation levels in OGD/R treated HT22 cells.** LDH release is an important indicator for detecting cell membrane integrity and is a widely used cell mortality assay. The results of the LDH assay showed that 20  $\mu\text{g/ml}$  RY-A (mortality of  $5.82 \pm 0.65\%$ ) significantly inhibited the amount of LDH release compared with that in the OGD/R group (mortality of  $14.69 \pm 0.97\%$ ), which resulted in a significant decrease in cell death ( $P < 0.0001$ ) as shown in Fig. 1D. The results related to oxidative levels showed that the levels of NO, ROS and MDA were significantly higher in the OGD/R group compared with the control group ( $P < 0.0001$ ). RY-A and EDA significantly reduced the levels of NO, ROS

and MDA compared with the OGD/R group; with a significant difference observed at 20  $\mu\text{g/ml}$  RY-A ( $P < 0.05$ ), as shown in Fig. 1E–G.

**Effect of RY-A on antioxidant levels in OGD/R treated HT22 cells.** The results relating to antioxidant levels showed that the activities of SOD and GSH-Px were significantly inhibited in the OGD/R group compared with the control group ( $P < 0.0001$ ). The EDA group had increased activities of SOD and GSH-Px compared with the OGD/R group ( $P < 0.0001$ ). Compared with the OGD/R group, RY-A 10 and 20  $\mu\text{g/ml}$  significantly elevated SOD activity ( $P < 0.0001$ ), whereas 40  $\mu\text{g/ml}$  RY-A did not significantly increase SOD activity. The activity of GSH-Px was significantly elevated in the RY-A group and 20  $\mu\text{g/ml}$  RY-A resulted in the highest GSH-Px activity ( $P < 0.0001$ ), as shown in Fig. 1H and I.

**Metabolomic analysis of OGD/R treated HT22 cells before and after RY-A treatment.** A total of 3,826 metabolites were identified by a combination of positive and negative ion modes. The cellular samples were analyzed using the validated UHPLC-MS method and after calibration and normalization, the data were imported into the R language Ropls package for PCA. Tight aggregation of quality control (QC) samples was observed in both positive and negative ion modes, indicating good stability and reproducibility of the instrument and method (Fig. 2A and C). The relative standard deviation (RSD) results of the QC samples showed that the number of characteristic peaks with  $\text{RSD} \leq 30\%$  in the QC samples accounted for more than 70% of the total characteristic peaks (Fig. 2B and D), indicating good data suitable for further analysis (13).

**Enrichment analysis of differential metabolites and their metabolic pathways.** The relationship between metabolite expression and sample category was first analyzed by PLS-DA. To avoid overfitting of the PLS-DA model during the modeling process, the replacement test was used to test the model and ensure its validity. The results showed that its  $R^2X$ ,  $R^2Y$  and  $Q^2$  values were 0.247, 0.998 and 0.681, respectively, for the positive ion model (Fig. 2E) and 0.302, 0.993 and 0.702, respectively, for the negative ion model (Fig. 2H), indicating that the constructed model was good without overfitting. As shown by PLS-DA (Fig. 2F and I), each sample in the OGD/R and RY-A groups showed a tendency of intra-group aggregation and inter-group dispersion. The PLS-DA model could distinguish between the two groups of samples, indicating that the administration of RY-A affected the metabolites in the OGD/R treated HT22 cells. Differential metabolites were screened by the OPLS-DA (Fig. 2G and J) to obtain VIP, which is used to illustrate the degree of contribution of the variables to the model, measuring the strength of the effect of differences in accumulation of each metabolite on the categorization and differentiation of samples in each group and the explanatory power. Differential metabolites with biological significance were mined. In the present study,  $\text{VIP} > 1$  and  $P < 0.05$  were used as screening criteria for significant differences in metabolites. A total of 20 metabolites were significantly different between the RY-A and OGD/R groups. Of these, five were upregulated: L-tryptophan, xanthine, uracil 5-carboxylic acid, guanidino-succinic acid and L-dopa.

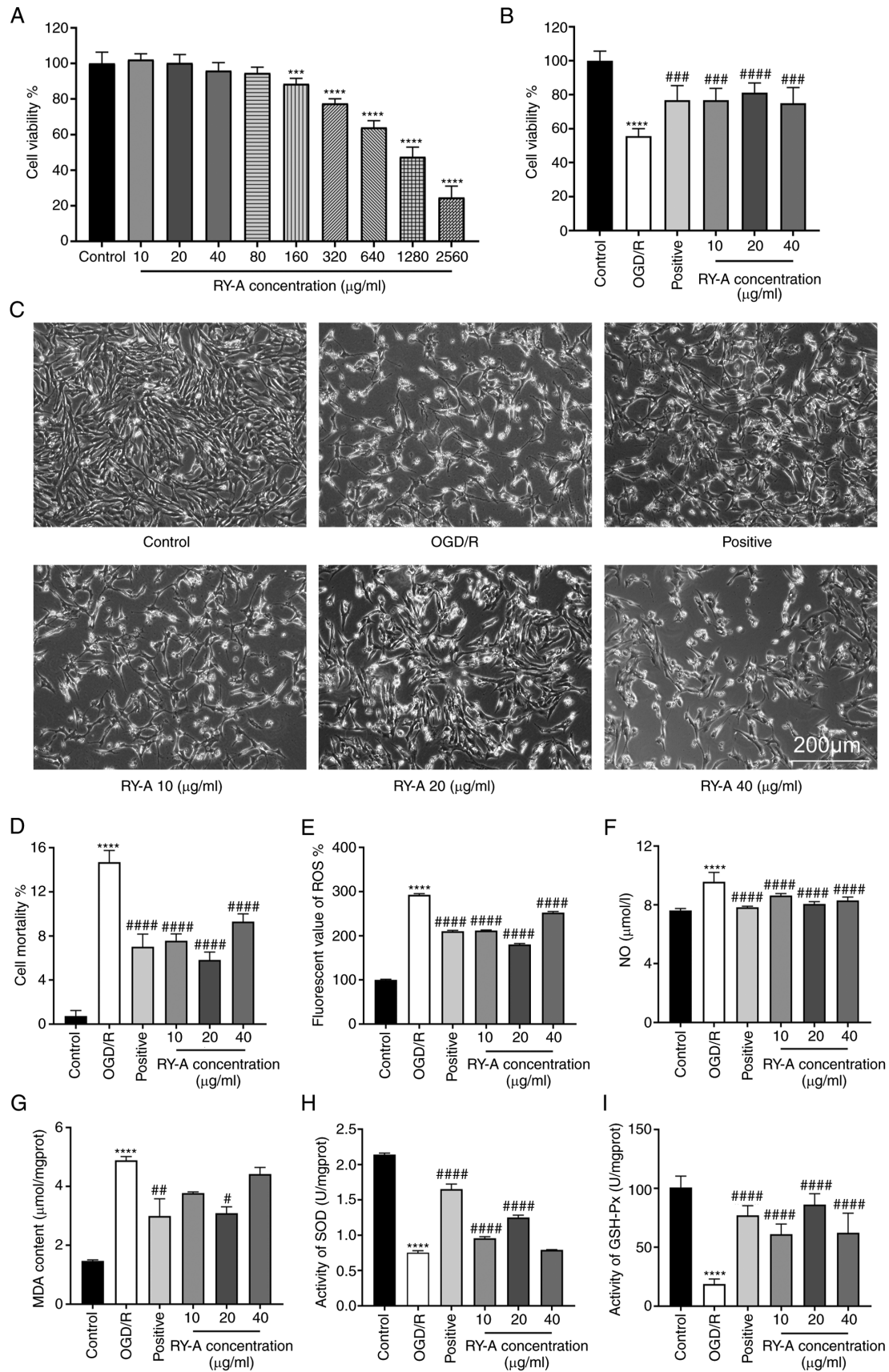


Figure 1 Cell safety of RY-A and effects of RY-A on cell viability, cell morphology, LDH release and oxidative stress in OGD/R-induced HT22 cells. (A) Effect of RY-A on the viability of HT22 cells. (B) Effect of RY-A on the viability of OGD/R-induced HT22 cells. (C) HT22 cell morphology in each group. (D) Detection of cellular mortality using the LDH cytotoxicity assay kit. Assay kits was used to detect (E) ROS and (F) NO. (G) Lipid oxidation assay kit was used to measure MDA. Assay kits was used to detect (H) SOD and (I) GSH-Px activity. Positive: EDA group, OGD/R + 100 μmol/l edaravone. Results were expressed as mean ± SD (n=6). \*\*\*P<0.001 and \*\*\*\*P<0.0001 vs. Control group #P<0.05, ##P<0.01, ###P<0.001 and ####P<0.0001 vs. OGD/R group. RY-A, *Rubia yunnanensis* alcohol extract; LDH, lactate dehydrogenase; OGD/R, oxygen-glucose deprivation/reoxygenation; ROS, reactive oxygen species; NO, nitric oxide; MDA SOD, superoxide dismutase; GSH-Px, glutathione peroxidase.

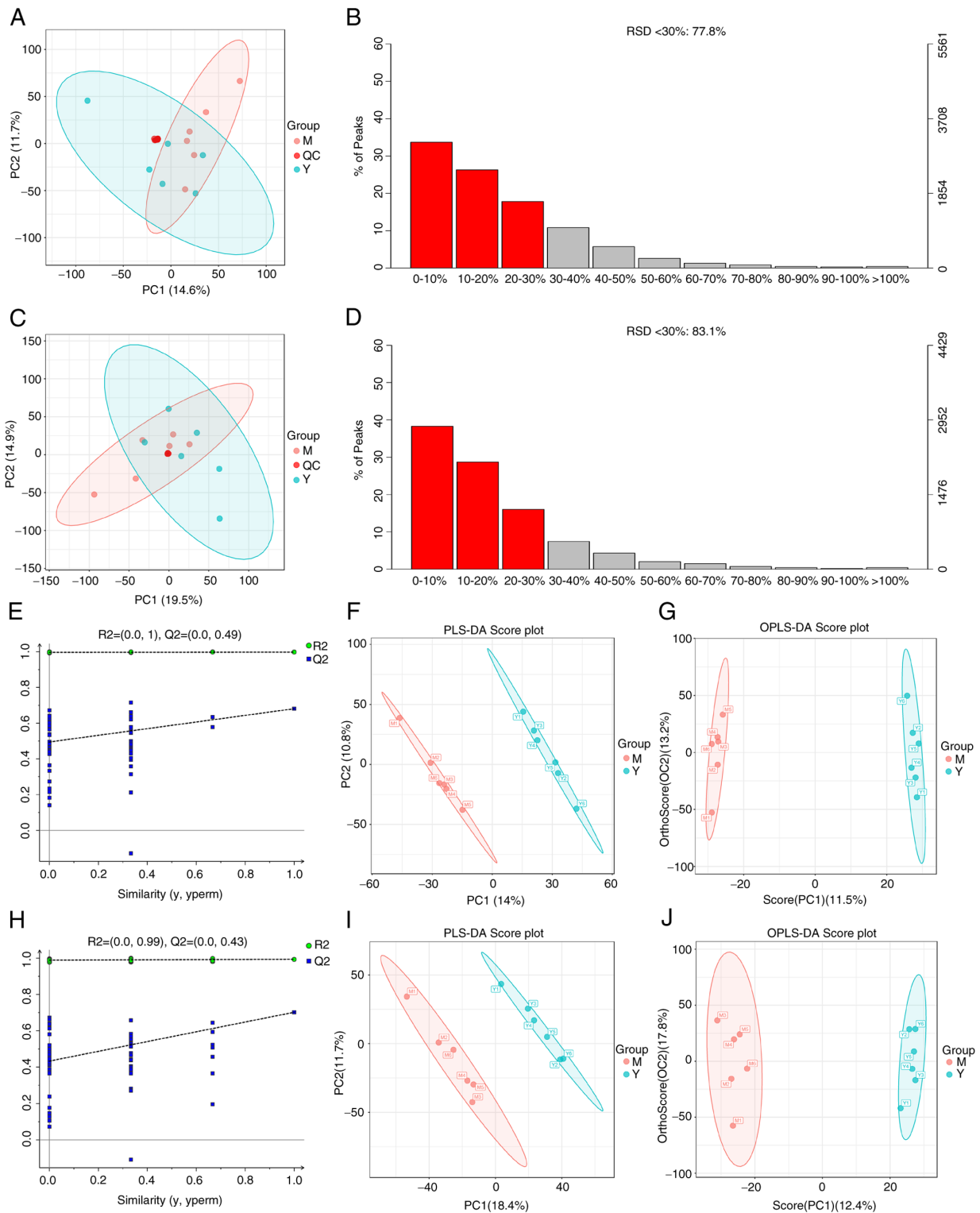


Figure 2. Instrument stability monitoring, validity analysis of the model and screening of differential metabolites. (A and C) PCA of cell samples and QC samples, in order of positive and negative ion PCA. (B and D) RSD analysis of QC samples, in order of positive and negative ion RSD. (E and H) The replacement test was used to verify whether the PLS-DA model was overfitted or not, in order of positive and negative ion replacement test. (F and I) PLS-DA of metabolic changes between samples from OGD/R group and RY-A group based on LC-MS/MS system, in order of positive ion and negative ion PLS-DA. (G and J) Screening of differential metabolites between OGD/R group and RY-A group using OPLS-DA, in order of Positive and negative ion OPLS-DA. PCA, principal component analysis; RSD, Relative Standard Deviation; QC, quality control; PLS-DA, partial least squares discriminant analysis; OGD/R, oxygen-glucose deprivation/reperfusion; RY-A, *Rubia yunnanensis* alcohol extract; OPLS-DA, orthogonal partial least squares discriminant analysis; M, OGD/R group; Y, RY-A group.

The other 15 metabolites were downregulated: ornithine, eicosapentaenoic acid-d5, isosafrole, inosine, adenosine 3'-monophosphate, 5'-methylthioadenosine, glycerol

3-phosphate, d-mannose, palmitoyl-L-carnitine, L-carnitine, cortexolone, L-cysteine, L-phenylalanine, shikimic acid, allocholic acid (Table I).

Table I. Screening results of differential metabolites in oxygen-glucose deprivation/reoxygenation group and *Rubia yunnanensis* alcohol extract group.

No.	Metabolite	Formula	m/z	RT(s)	Fold change	P-value	Variable projection importance	Electrospray ionization mode	Trend
1	L-Tryptophan	$C_{11}H_{12}N_2O_2$	205.098	193.045	0.941	$1.16 \times 10^{-3}$	2.585	[M+H] <sup>+</sup>	Up
2	Ornithine	$C_3H_{12}N_2O_2$	133.097	45.265	1.792	$1.82 \times 10^{-3}$	2.347	[M+H] <sup>+</sup>	Down
3	Eicosapentaenoic acid-d5	$C_{20}H_{30}O_2$	302.221	573.912	1.257	$2.52 \times 10^{-3}$	2.229	[M-H] <sup>-</sup>	Down
4	Isosafrole	$C_{10}H_{10}O_2$	163.076	533.436	1.112	$3.85 \times 10^{-3}$	2.224	[M+H] <sup>+</sup>	Down
5	Xanthine	$C_5H_4N_4O_2$	152.035	382.348	0.124	$4.51 \times 10^{-3}$	2.292	[M-H] <sup>-</sup>	Up
6	Inosine	$C_{10}H_{12}N_4O_5$	267.074	67.378	2.243	$1.02 \times 10^{-2}$	2.240	[M-H] <sup>-</sup>	Down
7	Adenosine 3'-monophosphate	$C_{10}H_{14}N_5O_7P$	348.070	53.845	2.194	$1.79 \times 10^{-2}$	1.969	[M+H] <sup>+</sup>	Down
8	Uracil 5-carboxylic acid	$C_5H_4N_2O_4$	156.966	145.502	0.367	$1.94 \times 10^{-2}$	1.938	[M+H] <sup>+</sup>	Up
9	5'-Methylthioadenosine	$C_{11}H_{15}N_5O_3S$	298.096	165.446	2.05	$2.04 \times 10^{-2}$	1.996	[M+H] <sup>+</sup>	Down
10	Glycerol 3-phosphate	$C_3H_9O_6P$	171.006	46.213	1.674	$2.10 \times 10^{-2}$	1.956	[M-H] <sup>-</sup>	Down
11	D-Mannose	$C_6H_{12}O_6$	179.988	686.854	1.281	$2.13 \times 10^{-2}$	1.936	[M-H] <sup>-</sup>	Down
12	Guanidino-succinic acid	$C_5H_9N_3O_4$	174.957	141.376	0.776	$2.31 \times 10^{-2}$	1.770	[M-H] <sup>-</sup>	Up
13	Palmitoyl-L-carnitine	$C_{23}H_{45}NO_4$	400.340	519.413	1.169	$2.41 \times 10^{-2}$	1.920	[M+H] <sup>+</sup>	Down
14	L-Carnitine	$C_7H_{15}NO_3$	162.112	51.576	1.837	$2.49 \times 10^{-2}$	1.846	[M+H] <sup>+</sup>	Down
15	Cortaxolone	$C_{21}H_{30}O_4$	346.331	461.884	1.54	$2.88 \times 10^{-2}$	1.885	[M+H] <sup>+</sup>	Down
16	L-Cysteine	$C_3H_7NO_2S$	122.019	44.167	2.181	$3.20 \times 10^{-2}$	1.781	[M+H] <sup>+</sup>	Down
17	L-Dopa	$C_9H_{11}NO_4$	196.000	59.143	0.553	$3.28 \times 10^{-2}$	1.844	[M-H] <sup>-</sup>	Up
18	L-Phenylalanine	$C_9H_{11}NO_2$	164.072	90.228	1.322	$3.31 \times 10^{-2}$	1.829	[M-H] <sup>-</sup>	Down
19	Shikimic acid	$C_7H_{10}O_5$	173.046	147.982	1.974	$3.70 \times 10^{-2}$	1.845	[M-H] <sup>-</sup>	Down
20	Allocholic acid	$C_{24}H_{40}O_5$	408.370	637.214	1.578	$4.04 \times 10^{-2}$	1.828	[M+H] <sup>+</sup>	Down

The row highlighted in red is the differential metabolite with the most significant change.

To more fully and visually analyze the differences between the OGD/R and RY-A groups, the relationships between the samples and differences in the accumulation of metabolites in different samples were demonstrated. Differential metabolites with  $FC > 1.5$  or  $< 0.67$  and  $P < 0.05$  were visualized as volcano plots (Fig. 3A). Selected metabolites were analyzed by clustering, with metabolites in the same cluster having similar accumulations and potentially similar functions or participation in the same metabolic processes or cellular pathways (Fig. 3B).

To observe overall alterations in metabolism, the present study captured the average and overall changes of all metabolites in pathways based on differential enrichment scores. As shown in Fig. 3C, the differential metabolites between the RY-A and OGD/R groups interacted with each other mainly through different pathways, such as 'phenylalanine, tyrosine and tryptophan biosynthesis', 'prolactin signaling pathway' and 'amphetamine addiction' and were collectively affecting body systems such as 'amino acid metabolism', 'endocrine system' and 'immune system'.

*Effect of RY-A treatment on indoleamine 2,3-dioxygenase (IDO) expression and MAPK signaling pathways.* The metabolite with the most significant difference following RY-A treatment was tryptophan. Indoleamine 2,3-dioxygenase is one of the major rate-limiting enzymes of the tryptophan-kynurenine pathway, which catalyzes the production of kynurenine from the essential amino acid L-tryptophan in mammalian extrahepatic tissues to exert an antioxidant effect (23). The signaling pathways of MAPKs (p38, ERK and JNK) have been highly correlated with oxidative stress-induced cell death (24-26). Also, an increase in kynurenine to tryptophan ratio after drug intervention in the metabolomics analysis of the present study implied elevated IDO activity (27). In the present study, western blotting was performed at two separate times to detect the expression levels of IDO proteins and major proteins of MAPK signaling pathways (p38, p-p38, ERK, p-ERK, JNK, p-JNK). Western blotting showed that the expression of IDO proteins was significantly downregulated and the phosphorylation of p-p38, p-ERK and p-JNK proteins was significantly upregulated in OGD/R treated HT22 cells compared with controls. In contrast, RY-A treatment enhanced OGD/R-induced expression of IDO in HT22 cells and attenuated the effect of OGD/R on the expression of major proteins of MAPK signaling pathways (Fig. 4A-F). These results suggest that RY-A may ameliorate ischemic injury in brain tissue by activating IDO protein expression and inhibiting the phosphorylation of MAPKs.

## Discussion

Our previous research used high-performance liquid chromatography to analyze the two main components, *Rubia yunnanensis* naphthoquinones A and *Rubia yunnanensis* quinone B, of the drug RY-A used in the present study (28). This analysis ensured that the quality of RY-A was up to standard. Mouse hippocampal neuron HT22 cells are widely used in the *in vitro* study of mechanisms of neurodegenerative disease (29). The present study investigated the neuroprotective effects of RY-A on HT22 cells by simulating

an *in vitro* CIRI model through OGD/R. Metabolic pathways underlying the effects of RY-A were examined by employing a metabolomics approach. It was found that OGD/R induced oxidative stress and reduced viability of HT22 cells by downregulating IDO enzyme activity and upregulating phosphorylation levels of MAPKs. The present study showed that 10-80  $\mu\text{g/ml}$  RY-A had no toxic effects on normal HT22 cells and tended to increase cell viability. Experiments to observe the effects of RY-A on the viability of OGD/R treated HT22 cells found that 10-20  $\mu\text{g/ml}$  RY-A dose-dependently increased cell viability, with 20  $\mu\text{g/ml}$  providing the optimal concentration. Further metabolomics analyses were performed with 20  $\mu\text{g/ml}$  RY-A.

OGD/R is closely associated with the aggravation of oxidative stress. The massive production of ROS with oxidative stress is one of the most critical aspects in the pathomechanisms of CIRI. Excessive oxidative stress also leads to lipid peroxidation as well as severe inflammation of neuronal cell membranes and organelles (30). The hallmark substances of oxidative stress include MDA, SOD and GSH-Px. The present study found that RY-A protected HT22 cells from OGD/R-induced oxidative damage and stress through the downregulation of ROS, NO and MDA oxidation products and the upregulation of SOD and GSH-Px antioxidant enzyme activities.

The metabolomics analysis showed that the protective effect of RY-A against OGD/R-induced cellular damage was mainly through affecting metabolites such as amino acids and their derivatives and organic acids. A total of 20 differential metabolites were obtained by comparative analysis of the RY-A and OGD/R groups, in which RY-A upregulated five metabolites (L-tryptophan, xanthine, uracil 5-carboxylic acid, guanidino-succinic acid and L-dopa) and downregulated 15 metabolites (ornithine, eicosapentaenoic acid-d5, isosafrole, inosine, adenosine 3'-monophosphate, 5'-methylthioadenosine, glycerol 3-phosphate, D-mannose, palmitoyl-L-carnitine, L-carnitine, cortexolone, L-cysteine, L-phenylalanine, shikimic acid and allocholic acid). Among them, L-tryptophan levels showed the most significant change. Tryptophan is an essential amino acid required for protein synthesis and >95% of free tryptophan is converted to kynurenine mainly by IDO and tryptophan-2,3-dioxygenase rate-limiting enzymes (31). Tryptophan metabolism has been associated with a variety of neurodegenerative diseases, including Alzheimer's disease and a metabolite of tryptophan, kynurenine, has a recognized neuroprotective effect (32-34). A review has shown that another metabolite of tryptophan, 5-hydroxytryptamine (serotonin), is involved in the regulation of neurological functions, such as behavior, mood and cognition (35). Supplementation of dietary tryptophan has a positive effect on neurodevelopment and improvement of sleep (36,37). Wang *et al.* (38) found that oral administration of tryptophan significantly improved depression and anxiety-like behaviors via the gut-brain-axis pathway in chronically and mildly stressed mice. Oğuz *et al.* (39) found that carotid artery infusion of tryptophan-containing histidine-tryptophan-ketoglutaric acid solution significantly reduced the degree of ischemia and the number of apoptotic cells in rabbits with CIRI and effectively enhanced the resistance of the brain to ischemic conditions.

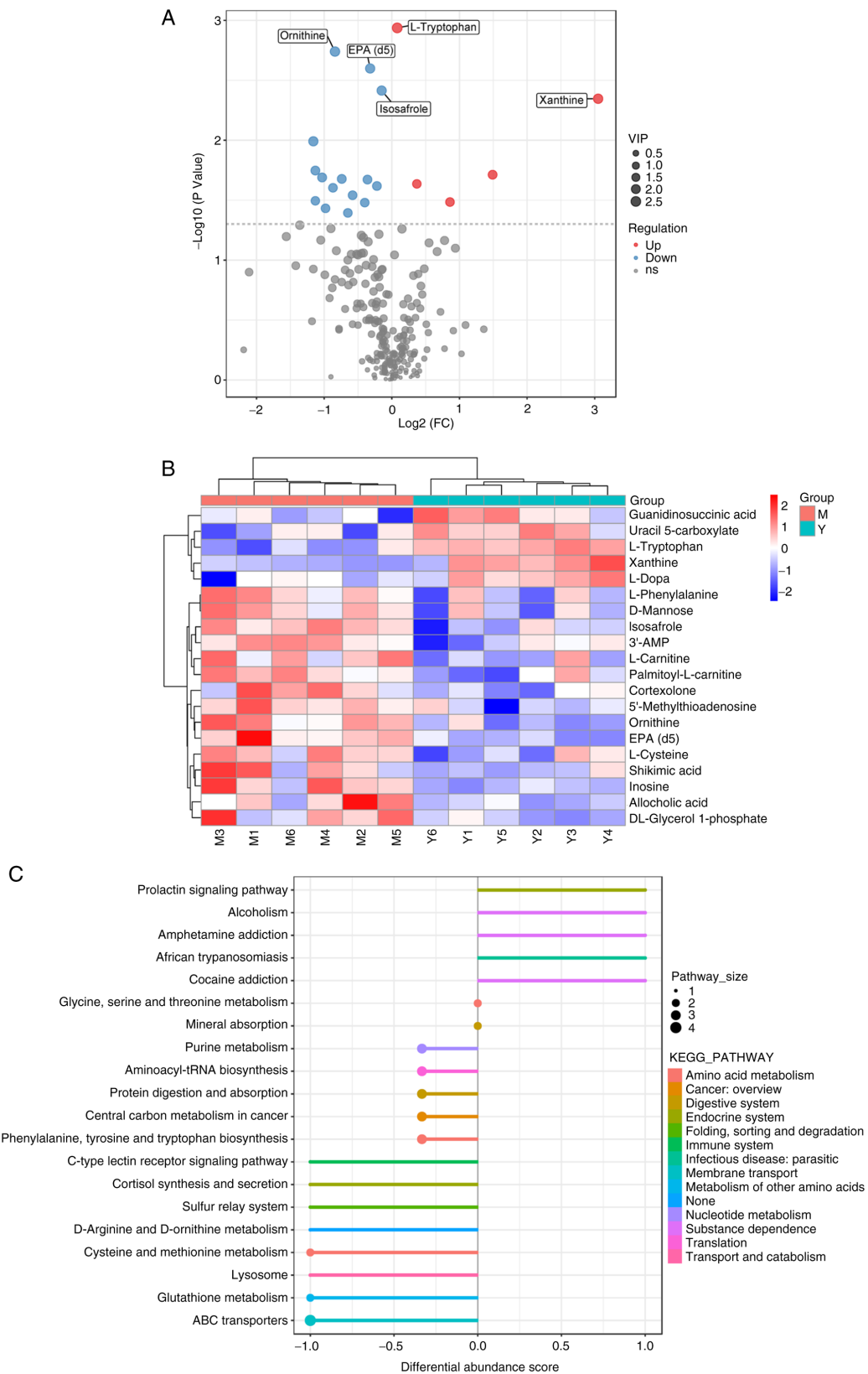


Figure 3. Enrichment analysis of differential metabolites and their metabolic pathways. (A) Differential metabolite volcano plot. The larger the absolute value of the horizontal coordinate, the larger the fold change in expression between the OGD/R group and the RY-A group. The larger the vertical coordinate value, the greater the statistical significance of its expression. Blue dots: downregulated metabolites, red dots: upregulated metabolites, gray dots: metabolites that did not meet the conditions of differential screening. The top five metabolite names with the smallest P-value are displayed by default. (B) Heatmap analysis of overall clustering of samples. The left clustering line is the metabolite clustering line and the top is the sample clustering line, the redder color indicates the higher expression level. (C) DA score plot of different metabolic pathways. The closer the score of a metabolic pathway is to 1.0, the more the overall expression of the pathway tends to be upregulated and vice versa, downregulated. The larger the dots are, the higher the number of metabolites contained. The color indicates the magnitude of the P-value, with redder reflecting a smaller P-value. OGD/R, oxygen-glucose deprivation/reperfusion; RY-A, *Rubia yunnanensis* alcohol extract; DA, differential abundance; OGD/R, oxygen-glucose deprivation/reperfusion; RY-A, *Rubia yunnanensis* alcohol extract; M, OGD/R group; Y, RY-A group.

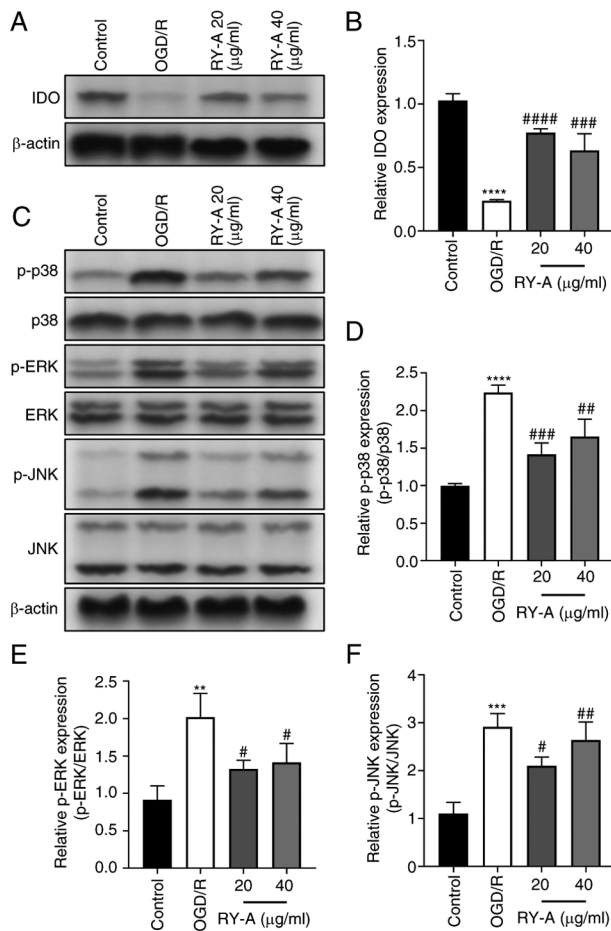


Figure 4. Effect of RY-A on IDO and MAPKs pathway protein expression in OGD/R-induced HT22 cells. Western blotting was performed to detect the expression of (A and B) IDO, (C and D) p-p38, (C and E) p-ERK, (C and F) p-JNK in OGD/R-induced HT22 cells and actin was used as a reference. Results are expressed as mean  $\pm$  SD (n=3). \*\*P<0.01, \*\*\*P<0.001 and \*\*\*\*P<0.0001 vs. Control group, \*P<0.05, \*\*P<0.01, \*\*\*P<0.001, \*\*\*\*P<0.0001 vs. OGD/R group. RY-A, *Rubia yunnanensis* alcohol extract; IDO, indoleamine 2,3-dioxygenase; OGD/R, oxygen-glucose deprivation/reperfusion; p-, phosphorylated.

Xanthine is a purine base commonly used as a mild stimulant. *In vitro* and *in vivo* studies have found that xanthine promotes the division and proliferation of mammary stem cells and enhances the activity of stem and progenitor cells (40,41). Guanidino-succinic acid, a constituent of normal urine, has been found to inhibit lipopolysaccharide-induced production of tumor necrosis factor- $\alpha$  by human monocytes, while the presence of 2-guanidino-succinic acid, methyl guanidine and guanidinoacetic acid limited the chemiluminescence produced by phorbol myristate acetate-treated HL-60 cells (42).

L-dopa is a hydroxylated form of complex amino acids that forms various catecholamines, such as dopamine, which is closely related to the modulation of neurological function. L-dopa pretreatment significantly attenuates dexamethasone-induced ischemia and promotes angiogenesis (43). L-dopa treatment increases the number of oligodendrocyte transcription factor 2-positive cells in the infarcted region of experimental animals and stimulates post-stroke plasticity (44). In addition, conversion of L-dopa to dopamine by decarboxylase inhibits H<sub>2</sub>O<sub>2</sub>-induced oxidative stress (45).

Ornithine is a nonprotein amino acid that serves as a core metabolite in the urea cycle. Zanatta *et al* (46) showed that ornithine treatment reduces the survival of astrocytes in the cerebral cortex and impairs mitochondrial function and antioxidant capacity of cells by decreasing mitochondrial membrane potential and GSH-Px concentrations. In addition, Fonteh *et al* (47) showed that increased ornithine in urine may serve as one of the biomarkers of Alzheimer's disease. Isosafrole, a natural product, has been evaluated as a Group III carcinogen by the International Agency for Research on Cancer (48). Adenosine 3'-monophosphate is a nucleotide that is reported to inhibit the proliferation of pro-glomerular vascular smooth muscle cells and thylakoid cells via either adenosine or A2B receptors (49). 5'-Methylthioadenosine is a sulfur-containing adenosine that is considered a tumor metabolite whose dysregulated metabolism negatively affects the immune function of a variety of immune cells, including T and NK cells (50). Glycerol 3-phosphate is an endogenous metabolite produced by the cytoplasmic glycerol 3-phosphate dehydrogenase pathway. Zhang *et al* (51) found that H<sub>2</sub>O<sub>2</sub>-induced oxidative stress in glucose medium increases glycerol 3-phosphate synthesis and stimulates the expression of glycerol kinase GlcA. D-Mannose is an important sugar involved in the glycosylation of several cellular molecules. A recent report (52) found that serum mannose levels can be used as an early biomarker for ovarian cancer. Palmitoyl-L-carnitine is a fatty acid metabolite. Recently, Guan *et al* (53) conducted the first clinical study using metabolomics and machine learning approaches and identified ornithine and palmitoyl-L-carnitine as potential biomarkers for screening lung cancer. Other research showed that an increase in palmitoyl-L-carnitine promotes fatty acid oxidation, which exacerbates oxidative stress and induces insulin resistance (54). Shikimic acid, a monomeric compound derived from anise, is reported to increase the risk of gastric and esophageal cancer (55-57). Ma and Ning (58) showed that shikimic acid promotes *in vitro* cell proliferation through the miR-300-mediated NF- $\kappa$ B pathway in MCF-7 and T47D cell models of breast cancer. Allocholic acid is a bile acid found in vertebrates. It has been found that patients with cirrhosis and brain tumors contain higher levels of allocholic acid compared with normal subjects (59,60). There appears to be no pharmacological studies related to uracil 5-carboxylic acid and only one chemical study of its enzymatic carboxylation has been reported (61). In summary, the underlying mechanisms of RY-A actions in the treatment of cerebral ischemia may be related to modulation of the aforementioned metabolites, in terms of anti-oxidant, anti-apoptotic and anti-inflammatory properties and the promotion of cell proliferation and angiogenesis.

The current study found that the metabolite with the most significant change in levels among the aforementioned metabolites was tryptophan, which plays a key role in cerebral ischemia. IDO enzymes are the main rate-limiting enzymes for tryptophan degradation (23). IDO enzymes consist of two members, IDO1 and IDO2. Studies have shown that overexpressed IDO proteins inhibits intracellular ROS levels and DNA damage in a rat model of ischemic injury and prevents neuronal cell death via free radical scavengers (62,63). Studies in models of certain cancers and neuronal diseases have also demonstrated that IDO expression exerts potent antioxidant functions, thereby significantly inhibiting

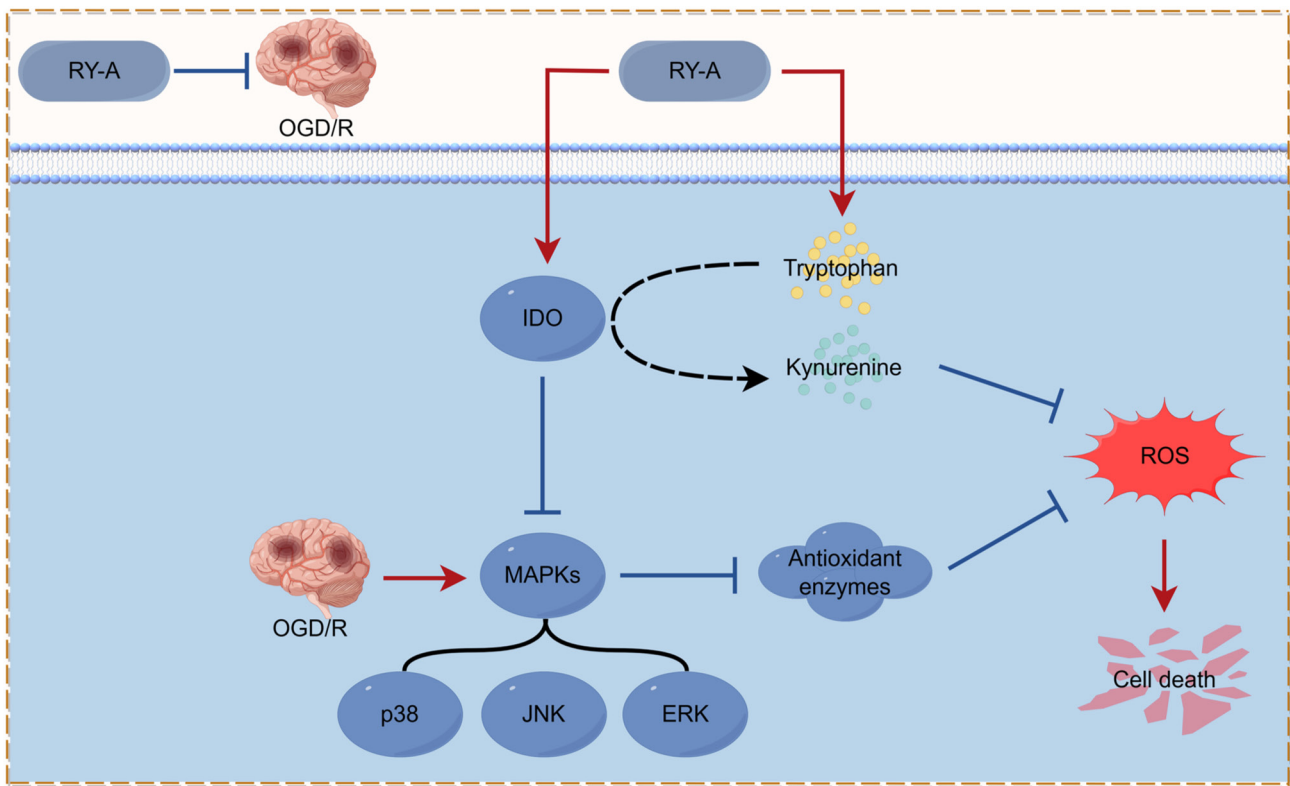


Figure 5 Overview of the mechanism of neuroprotective effect of RY-A on OGD/R-induced HT22 cells. The protective effect of RY-A may be related to the regulation of tryptophan metabolism and MAPKs signaling pathway (By Figdraw: www.figdraw.com). RY-A, *Rubia yunnanensis* alcohol extract; OGD/R, oxygen-glucose deprivation/reperfusion; IDO, indoleamine 2,3-dioxygenase; ROS, reactive oxygen species.

oxidative stress-induced cell death (64,65). In addition, it is well known that the MAPK (p38, ERK and JNK) signaling pathways are highly associated with oxidative stress-induced cell death (24-26). It has been reported that Tat-IDO-1 transduced into HT22 cells reduces cell death, ROS production, DNA fragmentation and H<sub>2</sub>O<sub>2</sub>-induced MAPK phosphorylation (23). Other studies have also shown that overexpression of IDO proteins inhibits the activation of MAPK signaling pathways under conditions of oxidative stress (66,67). Therefore, the present study investigated the mechanism by which RY-A increases tryptophan by examining the expression of IDO and MAPK pathway proteins. The current study showed that RY-A increased IDO protein expression levels and inhibited the protein phosphorylation of MAPKs (p38, ERK and JNK) in OGD/R treated HT22 cells, suggesting that RY-A may inhibit cerebral ischemia through IDO-mediated inhibition of MAPK phosphorylation.

Hashimoto *et al* (68) compared the differences in osteoarthritis (OA) development between lectin-like oxidized low-density lipoprotein receptor-1 (LOX-1) knockout mice and wild-type mice by replicating a mouse knee OA model of medial meniscus instability using LOX-1 knockout mice. They analyzed the expression of LOX-1 in articular cartilage and bone remnants by immunohistochemistry and double staining techniques and assessed the expression levels of molecular markers (e.g., Runt-related transcription factor 2 and type X collagen) associated with LOX-1. The findings revealed that LOX-1-deficient mice were resistant to osteoarthritis and also confirmed the involvement of the LOX-1/low-density

lipoprotein (oxLDL) system in cartilage degeneration and bone capsule formation in the development of OA (69,70). It was concluded that the binding of ox-LDL to LOX-1 increases the production of ROS, which subsequently causes oxidative stress (71). It is well known that various lifestyle-related diseases such as hyperlipidemia, hypertension, OA and diabetes involve oxidative stress and these conditions can lead to atherosclerosis via the LOX-1/ox-LDL system (68,72-74). Therefore, ROS will mainly affect those organs that contain a large amount of blood such as the liver (75), lungs (76), heart and brain (77), as well as tissues and organs that contain synovial fluid such as the joints, stomach (78), brain (79) and medulla oblongata (80).

In conclusion, the present study demonstrated the effectiveness of RY-A in treating HT22 cells in an *in vitro* OGD/R model and its possible molecular mechanisms. Following OGD/R-induced injury, RY-A significantly reduced the content of oxidized products such as ROS, NO and MDA and enhanced the activities of SOD and GSH-Px antioxidant enzymes, thus ameliorating damage from oxidative stress and reducing neuronal death. It was hypothesized that the neuroprotective effect of RY-A may be associated with regulation of the tryptophan metabolic pathway and MAPK signaling pathways during OGD/R (Fig. 5). These findings suggested that RY-A has some potential therapeutic value for patients with CIRI. The oxygen-glucose deprivation/reoxygenation (OGD/R) model is widely used for *ex vivo* studies of cerebral ischemia-reperfusion injury secondary to ischemic stroke. While neurons in the hippocampal region of the brain are

vulnerable sites of cerebral ischemia/reperfusion, they are commonly used in studies of cerebral ischemia/reperfusion injury. The HT22 cell line, an immortalized mouse hippocampal neuronal cell line, is a subclone of the mouse T4 cell line, which lacks an important receptor of the N-methyl-D-aspartic acid receptor, there is almost a consensus that HT22 cells are not excitable and this cell has rightly become one of the most commonly used *in vitro* cell models for oxidative stress-related studies (81,82). Therefore, the hippocampal neuron HT22 cells were selected as the main research object in the present study.

There are still some limitations to the present study, such as no animal-related *in vivo* experiments. RY-A is a crude extract and it is not known whether it also has a protective effect on cortex-associated neuronal cells and the efficacy of its main monomer constituents needs further in-depth study. Related studies on the major compounds in *Rubia yunnanensis* will be covered in subsequent studies by the group and follow-up studies may study relevant cells in the cortex.

### Acknowledgements

Not applicable.

### Funding

The present study was supported by the Xingdian Talent Support Program-Special for Young Talent (grant no. XDYC-QNRC-2022-0284), the High-level Talents Projects of Yunnan University of Chinese Medicine-Fifth Level Talents, the National Administration of Traditional Chinese Medicine High-level Key Discipline Construction Project 'Minority medicine (Dai Medicine)' (grant no. Zyyzdxk-2023193) and the Scientific Research Foundation of The Education Department of Yunnan Province (grant no. 2024Y372).

### Availability of data and materials

The data generated in the present study may be requested from the corresponding author. Metabolomics data have been deposited to the EMBL-EBI MetaboLights database (DOI: 10.1093/nar/gkad1045, PMID:37971328) with the identifier MTBLS9545 (URL: [www.ebi.ac.uk/metabolights/MTBLS9545](http://www.ebi.ac.uk/metabolights/MTBLS9545)).

### Authors' contributions

JC was the main contributor in writing the manuscript. JC, LY and XD designed the experiments. JC and GL were responsible for the statistical and data analysis. JC and XD drafted and revised the original manuscript. PC and GL confirmed the authenticity of all the original data. PC and XD interpreted the results of the study and gave the final approval for the forthcoming version. All authors read and approved the final manuscript.

### Ethics approval and consent to participate

Not applicable.

### Patient consent for publication

Not applicable.

### Competing interests

The authors declare that they have no competing interests.

### References

1. Lemmerman LR, Balch MHH, Moore JT, Alzate-Correa D, Rincon-Benavides MA, Salazar-Puerta A, Gnyawali S, Harris HN, Lawrence W, Ortega-Pineda L, *et al*: Nanotransfection-based vasculogenic cell reprogramming drives functional recovery in a mouse model of ischemic stroke. *Sci Adv* 7: eabd4735, 2021.
2. Mahmood A and Muir KW: Tenecteplase or alteplase: What is the thrombolytic agent of the future? *Curr Treat Options Neurol* 24: 503-513, 2022.
3. Bayraktutan U: Endothelial progenitor cells: Potential novel therapeutics for ischaemic stroke. *Pharmacol Res* 144: 181-191, 2019.
4. Mokin M, Ansari SA, McTaggart RA, Bulsara KR, Goyal M, Chen M and Fraser JF; Society of NeuroInterventional Surgery: Indications for thrombectomy in acute ischemic stroke from emergent large vessel occlusion (ELVO): Report of the SNIS standards and guidelines committee. *J Neurointerv Surg* 11: 215-220, 2019.
5. Banjara M and Ghosh C: Sterile neuroinflammation and strategies for therapeutic intervention. *Int J Inflamm* 2017: 8385961, 2017.
6. Gülke E, Gelderblom M and Magnus T: Danger signals in stroke and their role on microglia activation after ischemia. *Ther Adv Neurol Disord* 11: 1756286418774254, 2018.
7. Jurcau A and Ardelean IA: Molecular pathophysiological mechanisms of ischemia/reperfusion injuries after recanalization therapy for acute ischemic stroke. *J Integr Neurosci* 20: 727-744, 2021.
8. Xu JY, Liu FY, Liu SX, Xie LZ, Li J, Ma YT and Han FJ: Plant-derived Chinese medicine monomers on ovarian cancer via the Wnt/ $\beta$ -catenin signaling pathway: Review of mechanisms and prospects. *J Oncol* 2021: 6852867, 2021.
9. Yi S, Lin Q, Zhang X, Wang J, Miao Y and Tan N: Selection and validation of appropriate reference genes for quantitative RT-PCR analysis in *Rubia yunnanensis* diels based on transcriptome data. *Biomed Res Int* 2020: 5824841, 2020.
10. Zhang R, Miao Y, Chen L, Yi S and Tan N: De novo transcriptome analysis reveals putative genes involved in anthraquinone biosynthesis in *Rubia yunnanensis*. *Genes (Basel)* 13: 521, 2022.
11. Luo L, Lü L, Lu Y, Zhang L, Li B, Guo K, Chen L, Wang Y, Shao Y and Xu J: Effects of hypoxia on progranulin expression in HT22 mouse hippocampal cells. *Mol Med Rep* 9: 1675-1680, 2014.
12. Zelena E, Dunn WB, Broadhurst D, Francis-McIntyre S, Carroll KM, Begley P, O'Hagan S, Knowles JD and Halsall A; HUSERMET Consortium; Wilson ID, Kell DB: Development of a robust and repeatable UPLC-MS method for the long-term metabolomic study of human serum. *Anal Chem* 81: 1357-1364, 2009.
13. Want EJ, Masson P, Michopoulos F, Wilson ID, Theodoridis G, Plumb RS, Shockcor J, Loftus N, Holmes E and Nicholson JK: Global metabolic profiling of animal and human tissues via UPLC-MS. *Nat Protoc* 8: 17-32, 2013.
14. Rasmussen JA, Villumsen KR, Ernst M, Hansen M, Forberg T, Gopalakrishnan S, Gilbert MTP, Bojesen AM, Kristiansen K and Limborg MT: A multi-omics approach unravels metagenomic and metabolic alterations of a probiotic and synbiotic additive in rainbow trout (*Oncorhynchus mykiss*). *Microbiome* 10: 21, 2022.
15. Navarro-Reig M, Jaumot J, Garcia-Reiriz A and Tauler R: Evaluation of changes induced in rice metabolome by Cd and Cu exposure using LC-MS with XCMS and MCR-ALS data analysis strategies. *Anal Bioanal Chem* 407: 8835-8847, 2015.
16. Wishart DS, Tzur D, Knox C, Eisner R, Guo AC, Young N, Cheng D, Jewell K, Arndt D, Sawhney S, *et al*: HMDB: The human metabolome database. *Nucleic Acids Res* 35 (Database Issue): D521-D526, 2007.

17. Horai H, Arita M, Kanaya S, Nihei Y, Ikeda T, Suwa K, Ojima Y, Tanaka K, Tanaka S, Aoshima K, *et al*: MassBank: A public repository for sharing mass spectral data for life sciences. *J Mass Spectrom* 45: 703-714, 2010.
18. Sud M, Fahy E, Cotter D, Brown A, Dennis EA, Glass CK, Merrill AH Jr, Murphy RC, Raetz CR, Russell DW and Subramaniam S: LMSD: LIPID MAPS structure database. *Nucleic Acids Res* 35 (Database Issue): D527-D532, 2007.
19. Abdelrazig S, Safo L, Rance GA, Fay MW, Theodosiou E, Topham PD, Kim DH and Fernández-Castané A: Metabolic characterisation of *Magnetospirillum gryphiswaldense* MSR-1 using LC-MS-based metabolite profiling. *RSC Adv* 10: 32548-32560, 2020.
20. Ogata H, Goto S, Sato K, Fujibuchi W, Bono H and Kanehisa M: KEGG: Kyoto encyclopedia of genes and genomes. *Nucleic Acids Res* 27: 29-34, 1999.
21. Thévenot EA, Roux A, Xu Y, Ezan E and Junot C: Analysis of the human adult urinary metabolome variations with age, body mass index, and gender by implementing a comprehensive workflow for univariate and OPLS statistical analyses. *J Proteome Res* 14: 3322-3335, 2015.
22. Xia J and Wishart DS: Web-based inference of biological patterns, functions and pathways from metabolomic data using MetaboAnalyst. *Nat Protoc* 6: 743-760, 2011.
23. Park JH, Kim DW, Shin MJ, Park J, Han KH, Lee KW, Park JK, Choi YJ, Yeo HJ, Yeo EJ, *et al*: Tat-indoleamine 2,3-dioxygenase 1 elicits neuroprotective effects on ischemic injury. *BMB Rep* 53: 582-587, 2020.
24. Jia L, Chen Y, Tian YH and Zhang G: MAPK pathway mediates the anti-oxidative effect of chicoric acid against cerebral ischemia-reperfusion injury in vivo. *Exp Ther Med* 15: 1640-1646, 2018.
25. Kwon SH, Hong SI, Kim JA, Jung YH, Kim SY, Kim HC, Lee SY and Jang CG: The neuroprotective effects of *Lonicera japonica* THUNB. Against hydrogen peroxide-induced apoptosis via phosphorylation of MAPKs and PI3K/Akt in SH-SY5Y cells. *Food Chem Toxicol* 49: 1011-1019, 2011.
26. Zhu N, Cai C, Zhou A, Zhao X, Xiang Y and Zeng C: Schisandrin B prevents hind limb from ischemia-reperfusion-induced oxidative stress and inflammation via MAPK/NF- $\kappa$ B pathways in rats. *Biomed Res Int* 2017: 4237973, 2017.
27. Mallik SB, Mudgal J, Kinra M, Hall S, Grant GD, Anoopkumar-Dukie S, Nampoothiri M, Zhang Y and Arora D: Involvement of indoleamine 2,3-dioxygenase (IDO) and brain-derived neurotrophic factor (BDNF) in the neuroprotective mechanisms of ferulic acid against depressive-like behaviour. *Metab Brain Dis* 38: 2243-2254, 2023.
28. Li G, Cheng J, Yang L, Chen P and Duan X: Ethanol extract of *Rubia yunnanensis* inhibits carotid atherosclerosis via the PI3K/AKT signaling pathway. *Biomed Rep* 20: 19, 2023.
29. Zhao J, Liu L, Zhang L, Lv J, Guo X, Li X and Zhao T: Sodium ferulate attenuates high-glucose-induced oxidative injury in HT22 hippocampal cells. *Exp Ther Med* 18: 2015-2020, 2019.
30. Li S, Jiang D, Ehlerding EB, Rosenkrans ZT, Engle JW, Wang Y, Liu H, Ni D and Cai W: Intrathecal administration of nanoclusters for protecting neurons against oxidative stress in cerebral ischemia/reperfusion injury. *ACS Nano* 13: 13382-13389, 2019.
31. Pathakoti K, Goodla L, Manubolu M and Tenconmao T: Metabolic alterations and the protective effect of punicalagin against glutamate-induced oxidative toxicity in HT22 cells. *Neurotox Res* 31: 521-531, 2017.
32. Kincses ZT, Toldi J and Vécsei L: Kynurenines, neurodegeneration and Alzheimer's disease. *J Cell Mol Med* 14: 2045-2054, 2010.
33. Campesan S, Green EW, Breda C, Sathyasaikumar KV, Muchowski PJ, Schwarcz R, Kyriacou CP and Giorgini F: The kynurenine pathway modulates neurodegeneration in a *Drosophila* model of Huntington's disease. *Curr Biol* 21: 961-966, 2011.
34. Meier-Stephenson FS, Meier-Stephenson VC, Carter MD, Meek AR, Wang Y, Pan L, Chen Q, Jacobo S, Wu F, Lu E, *et al*: Alzheimer's disease as an autoimmune disorder of innate immunity endogenously modulated by tryptophan metabolites. *Alzheimers Dement (N Y)* 8: e12283, 2022.
35. Roth W, Zadeh K, Vekariya R, Ge Y and Mohamadzadeh M: Tryptophan metabolism and gut-brain homeostasis. *Int J Mol Sci* 22: 2973, 2021.
36. Carhart-Harris RL and Nutt DJ: Serotonin and brain function: A tale of two receptors. *J Psychopharmacol* 31: 1091-1120, 2017.
37. Cowen P and Sherwood AC: The role of serotonin in cognitive function: Evidence from recent studies and implications for understanding depression. *J Psychopharmacol* 27: 575-583, 2013.
38. Wang D, Wu J, Zhu P, Xie H, Lu L, Bai W, Pan W, Shi R, Ye J, Xia B, *et al*: Tryptophan-rich diet ameliorates chronic unpredictable mild stress induced depression- and anxiety-like behavior in mice: The potential involvement of gut-brain axis. *Food Res Int* 157: 111289, 2022.
39. Oğuz S, Aşgün HF and Büyük B: Effectiveness of brain protection with histidine-tryptophan-ketoglutarate solutions. *Heart Surg Forum* 23: E510-E516, 2020.
40. Deng WW and Ashihara H: Profiles of purine metabolism in leaves and roots of *Camellia sinensis* seedlings. *Plant Cell Physiol* 51: 2105-2118, 2010.
41. Kawasaki H, Shimaoka M, Usuda Y and Utagawa T: End-product regulation and kinetic mechanism of guanosine-inosine kinase from *Escherichia coli*. *Biosci Biotechnol Biochem* 64: 972-979, 2000.
42. Glorieux GL, Dhondt AW, Jacobs P, Van Langeraert J, Lameire NH, De Deyn PP and Vanholder RC: In vitro study of the potential role of guanidines in leukocyte functions related to atherogenesis and infection. *Kidney Int* 65: 2184-2192, 2004.
43. Price CF, Burgess DJ and Kastellorizios M: L-DOPA as a small molecule surrogate to promote angiogenesis and prevent dexamethasone-induced ischemia. *J Control Release* 235: 176-181, 2016.
44. Talhada D, Marklund N, Wieloch T, Kuric E and Ruscher K: Plasticity-enhancing effects of levodopa treatment after stroke. *Int J Mol Sci* 22: 10226, 2021.
45. Lotsios NS, Arvanitis N, Charonitakis AG, Mpekoulis G, Frakolaki E, Vassilaki N, Sideris DC and Vassilacopoulou D: Expression of human L-dopa decarboxylase (DDC) under conditions of oxidative stress. *Curr Issues Mol Biol* 45: 10179-10192, 2023.
46. Zanatta A, Rodrigues MDN, Amaral AU, Souza DG, Quincozes-Santos A and Wajner M: Ornithine and homocitrulline impair mitochondrial function, decrease antioxidant defenses and induce cell death in menadione-stressed rat cortical astrocytes: Potential mechanisms of neurological dysfunction in HHH syndrome. *Neurochem Res* 41: 2190-2198, 2016.
47. Fonteh AN, Harrington RJ, Tsai A, Liao P and Harrington MG: Free amino acid and dipeptide changes in the body fluids from Alzheimer's disease subjects. *Amino Acids* 32: 213-224, 2007.
48. No authors listed: Overall evaluations of carcinogenicity: An updating of IARC Monographs volumes 1 to 42. *IARC Monogr Eval Carcinog Risks Hum Suppl* 7: 1-440, 1987.
49. Zschocke S, Heidrich V and Kuhlmann E: Mapping the spontaneous EEG in focal disorders. *EEG EMG Z Elektroenzephalogr Elektromyogr Verwandte Geb* 21: 233-242, 1990 (In German).
50. Jacobs B, Schlögl S, Strobl CD, Völkl S, Stoll A, Mougiakakos D, Malmberg KJ, Mackensen A and Aigner M: The Oncometabolite 5'-deoxy-5'-methylthioadenosine blocks multiple signaling pathways of nk cell activation. *Front Immunol* 11: 2128, 2020.
51. Zhang C, Gu H, Ren Y and Lu L: GlcA-mediated glycerol-3-phosphate synthesis contributes to the oxidation resistance of *Aspergillus fumigatus* via decreasing the cellular ROS. *Fungal Genet Biol* 149: 103531, 2021.
52. Chen Y, Yao Q, Zhang L and Zeng P: HPLC for simultaneous quantification of free mannose and glucose concentrations in serum: Use in detection of ovarian cancer. *Front Chem* 11: 1289211, 2023.
53. Guan X, Du Y, Ma R, Teng N, Ou S, Zhao H and Li X: Construction of the XGBoost model for early lung cancer prediction based on metabolic indices. *BMC Med Inform Decis Mak* 23: 107, 2023.
54. Turnbull PC, Dehghani AC, Theriault CF, Connor MK and Perry CGR: Synergistic activation of mitochondrial metabolism and the glutathione redox couple protects HepG2 hepatocarcinoma cells from palmitoylecarnitine-induced stress. *Am J Physiol Cell Physiol* 317: C1324-C1329, 2019.
55. Brown AC: Cancer related to herbs and dietary supplements: Online table of case reports. Part 5 of 5. *J Diet Suppl* 15: 556-581, 2018.
56. Jones RS, Ali M, Ioannides C, Styles JA, Ashby J, Sulej J and Parke DV: The mutagenic and cell transforming properties of shikimic acid and some of its bacterial and mammalian metabolites. *Toxicol Lett* 19: 43-50, 1983.
57. Stavric B and Stoltz DR: Shikimic acid. *Food Cosmet Toxicol* 14: 141-145, 1976.

58. Ma X and Ning S: Shikimic acid promotes estrogen receptor(ER)-positive breast cancer cells proliferation via activation of NF- $\kappa$ B signaling. *Toxicol Lett* 312: 65-71, 2019.
59. Fine JM, Vrieze LA and Sorensen PW: Evidence that petromyzontid lampreys employ a common migratory pheromone that is partially comprised of bile acids. *J Chem Ecol* 30: 2091-2110, 2004.
60. Ohdoi C, Nyhan WL and Kuhara T: Chemical diagnosis of Lesch-Nyhan syndrome using gas chromatography-mass spectrometry detection. *J Chromatogr B Analyt Technol Biomed Life Sci* 792: 123-130, 2003.
61. Palmatier RD, McCroskey RP and Abbott MT: The enzymatic conversion of uracil 5-carboxylic acid to uracil and carbon dioxide. *J Biol Chem* 245: 6706-6710, 1970.
62. Liu H, Liu L and Visner GA: Nonviral gene delivery with indoleamine 2,3-dioxygenase targeting pulmonary endothelium protects against ischemia-reperfusion injury. *Am J Transplant* 7: 2291-2300, 2007.
63. Taguchi A, Hara A, Saito K, Hoshi M, Niwa M, Seishima M and Mori H: Localization and spatiotemporal expression of IDO following transient forebrain ischemia in gerbils. *Brain Res* 1217: 78-85, 2008.
64. Freewan M, Rees MD, Plaza TSS, Glaros E, Lim YJ, Wang XS, Yeung AW, Witting PK, Terentis AC and Thomas SR: Human indoleamine 2,3-dioxygenase is a catalyst of physiological heme peroxidase reactions: Implications for the inhibition of dioxygenase activity by hydrogen peroxide. *J Biol Chem* 288: 1548-1567, 2013.
65. Taniguchi T, Sono M, Hirata F, Hayaishi O, Tamura M, Hayashi K, Iizuka T and Ishimura Y: Indoleamine 2,3-dioxygenase. Kinetic studies on the binding of superoxide anion and molecular oxygen to enzyme. *J Biol Chem* 254: 3288-3294, 1979.
66. Grant RS, Naif H, Espinosa M and Kapoor V: IDO induction in IFN-gamma activated astroglia: A role in improving cell viability during oxidative stress. *Redox Rep* 5: 101-104, 2000.
67. Guillemain GJ, Smythe G, Takikawa O and Brew BJ: Expression of indoleamine 2,3-dioxygenase and production of quinolinic acid by human microglia, astrocytes, and neurons. *Glia* 49: 15-23, 2005.
68. Hashimoto K, Mori S, Oda Y, Nakano A, Sawamura T and Akagi M: Lectin-like oxidized low density lipoprotein receptor 1-deficient mice show resistance to instability-induced osteoarthritis. *Scand J Rheumatol* 45: 412-422, 2016.
69. Akagi M, Kanata S, Mori S, Itabe H, Sawamura T and Hamanishi C: Possible involvement of the oxidized low-density lipoprotein/lectin-like oxidized low-density lipoprotein receptor-1 system in pathogenesis and progression of human osteoarthritis. *Osteoarthritis Cartilage* 15: 281-290, 2007.
70. Hashimoto K, Oda Y, Nakamura F, Kakinoki R and Akagi M: Lectin-like, oxidized low-density lipoprotein receptor-1-deficient mice show resistance to age-related knee osteoarthritis. *Eur J Histochem* 61: 2762, 2017.
71. Kattoor AJ, Pothineni NVK, Palagiri D and Mehta JL: Oxidative stress in atherosclerosis. *Curr Atheroscler Rep* 19: 42, 2017.
72. Mitra S, Deshmukh A, Sachdeva R, Lu J and Mehta JL: Oxidized low-density lipoprotein and atherosclerosis implications in anti-oxidant therapy. *Am J Med Sci* 342: 135-142, 2011.
73. Li X, Tang X, Liu B, Zhang J, Zhang Y, Lv H, Liu D, Mehta JL and Wang X: LOX-1 deletion attenuates myocardial fibrosis in the aged mice, particularly those with hypertension. *Front Cardiovasc Med* 8: 736215, 2021.
74. Qiu J, Liu J, Tian L, Yu J, Duan Q, Liu Y, Zhao W, Si H, Lu X and Zhang Q: Knockdown of LOX-1 ameliorates bone quality and generation of type H blood vessels in diabetic mice. *Arch Biochem Biophys* 752: 109870, 2024.
75. Paradies G, Paradies V, Ruggiero FM and Petrosillo G: Oxidative stress, cardiolipin and mitochondrial dysfunction in nonalcoholic fatty liver disease. *World J Gastroenterol* 20: 14205-14218, 2014.
76. Valavanidis A, Vlachogianni T, Fiotakis K and Loridas S: Pulmonary oxidative stress, inflammation and cancer: Respirable particulate matter, fibrous dusts and ozone as major causes of lung carcinogenesis through reactive oxygen species mechanisms. *Int J Environ Res Public Health* 10: 3886-3907, 2013.
77. Songbo M, Lang H, Xinyong C, Bin X, Ping Z and Liang S: Oxidative stress injury in doxorubicin-induced cardiotoxicity. *Toxicol Lett* 307: 41-48, 2019.
78. Chen X, Zhao Y, Luo W, Chen S, Lin F, Zhang X, Fan S, Shen X, Wang Y and Liang G: Celastrol induces ROS-mediated apoptosis via directly targeting peroxiredoxin-2 in gastric cancer cells. *Theranostics* 10: 10290-10308, 2020.
79. Jimenez-Blasco D, Almeida A and Bolaños JP: Brightness and shadows of mitochondrial ROS in the brain. *Neurobiol Dis* 184: 106199, 2023.
80. Braga VA, Colombari E and Jovita MG: Angiotensin II-derived reactive oxygen species underpinning the processing of the cardiovascular reflexes in the medulla oblongata. *Neurosci Bull* 27: 269-274, 2011.
81. Majrashi M, Altukri M, Ramesh S, Govindarajulu M, Schwartz J, Almaghrabi M, Smith F, Thomas T, Suppiramaniam V, Moore T, *et al*:  $\beta$ -hydroxybutyric acid attenuates oxidative stress and improves markers of mitochondrial function in the HT-22 hippocampal cell line. *J Integr Neurosci* 20: 321-329, 2021.
82. Yan W, Guo T, Liu N, Cui X, Wei X, Sun Y, Hu H and Chen L: Erythropoietin ameliorates cognitive deficits by improving hippocampal and synaptic damage in streptozotocin-induced diabetic mice. *Cell Signal* 106: 110614, 2023.



Copyright © 2024 Cheng et al. This work is licensed under a Creative Commons Attribution-NonCommercial-NoDerivatives 4.0 International (CC BY-NC-ND 4.0) License.